



HAL
open science

Magnesium Partitioning Between Earth's Mantle and Core and its Potential to Drive an Early Exsolution Geodynamo

James Badro, Julien Aubert, Kei Hirose, Ryuichi Nomura, Ingrid Blanchard, Stephan Borensztajn, Julien Siebert

► **To cite this version:**

James Badro, Julien Aubert, Kei Hirose, Ryuichi Nomura, Ingrid Blanchard, et al.. Magnesium Partitioning Between Earth's Mantle and Core and its Potential to Drive an Early Exsolution Geodynamo. *Geophysical Research Letters*, 2018, 45 (24), pp.13,240-13,248. 10.1029/2018GL080405 . hal-02129830

HAL Id: hal-02129830

<https://hal.science/hal-02129830>

Submitted on 15 May 2019

HAL is a multi-disciplinary open access archive for the deposit and dissemination of scientific research documents, whether they are published or not. The documents may come from teaching and research institutions in France or abroad, or from public or private research centers.

L'archive ouverte pluridisciplinaire **HAL**, est destinée au dépôt et à la diffusion de documents scientifiques de niveau recherche, publiés ou non, émanant des établissements d'enseignement et de recherche français ou étrangers, des laboratoires publics ou privés.



RESEARCH LETTER

10.1029/2018GL080405

Key Points:

- A new thermodynamic model of magnesium metal-silicate partitioning is proposed, fitting all previously published data along with 22 new experiments
- MgO, not Mg, dissolves into iron; partitioning depends on T and metal composition, and is independent of P and silicate composition
- MgO exsolution during Earth's core cooling ($\sim 10^{-6} \text{ K}^{-1}$) produces a buoyancy flux on the order of 105 kg/s, able to generate a dipolar magnetic field of 40–70 μT

Supporting Information:

- Supporting Information S1
- Data Set S1
- Data Set S2
- Data Set S3

Correspondence to:

J. Badro,
badro@ipgp.fr

Citation:

Badro, J., Aubert, J., Hirose, K., Nomura, R., Blanchard, I., Borensztajn, S., & Siebert, J. (2018). Magnesium partitioning between Earth's mantle and core and its potential to drive an early exsolution geodynamo.

Geophysical Research Letters, 45. <https://doi.org/10.1029/2018GL080405>

Received 7 SEP 2018

Accepted 30 NOV 2018

Accepted article online 3 DEC 2018

Magnesium Partitioning Between Earth's Mantle and Core and its Potential to Drive an Early Exsolution Geodynamo

James Badro^{1,2} , Julien Aubert¹, Kei Hirose^{3,4} , Ryuichi Nomura⁵, Ingrid Blanchard¹ ,
Stephan Borensztajn¹, and Julien Siebert^{1,6}

¹Institut de physique du globe de Paris, Université de Paris, France, ²Earth and Planetary Science Laboratory, École Polytechnique Fédérale de Lausanne, Switzerland, ³Earth and Planetary Science, The University of Tokyo, Japan, ⁴ELSI, Tokyo Institute of Technology, Japan, ⁵Geodynamics Research Center, Ehime University, Japan, ⁶Institut Universitaire de France, France

Abstract Magnesium partitioning between metal and silicate was experimentally investigated between 34 and 138 GPa, 3,500 and 5,450 K using laser-heated diamond anvil cells. The 22 measurements are combined with previously published data (total of 49 measurements) to model magnesium metal-silicate partitioning using a thermodynamically consistent framework based on the interaction parameter formalism. The observations support the mechanism of MgO dissolution in the metal, ruling out other mechanisms. The magnesium partition coefficient depends on temperature and metal composition, but not on pressure or silicate composition. The equilibrium concentration and the exsolution rate of MgO in Earth's core can therefore be calculated for any P, T, and composition. Using a core thermal evolution model, the buoyancy flux converts to a magnetic field at Earth's surface, with dipole intensities between 40 and 70 μT prior to inner core growth, consistent with the paleomagnetic record going back to the Archean.

Plain Language Summary We measure the incorporation of magnesium oxide (one of the main components of Earth's mantle) into iron (the main constituent Earth's core), using extremely high pressure and temperature experiments that mimic the conditions of Earth's mantle and core. We find that magnesium oxide dissolution depends on temperature but not on pressure, and on metal (i.e., core) composition but not silicate (i.e., mantle) composition. Our findings support the idea that magnesium oxide dissolved in the core during its formation will precipitate out during subsequent core cooling. The precipitation should stir the entire core to produce a magnetic field in Earth's distant past, at least as intense as the present-day field.

1. Introduction

Thermal and dynamical models of Earth's core stipulate that the present-day geodynamo is powered by compositional buoyancy due to inner core growth (Buffett et al., 1996; Gubbins et al., 2003; Labrosse, 2015; Labrosse et al., 1997). Since the paleomagnetic record traces the existence of a magnetic field at least as early as 3.45 Gyr ago (Tarduno et al., 2010), and because estimates of the age of the inner core are younger than that (Biggin et al., 2015; Labrosse, 2015; Pozzo et al., 2012), an alternative source is required to power an early geodynamo prior to inner core growth.

The exsolution (or precipitation) of magnesium from Earth's core was recently proposed (O'Rourke & Stevenson, 2016) as a mechanism causing compositional buoyancy in core prior to inner core growth, with the potential to drive a dynamo. Recent experimental evidence (Badro et al., 2016) reported magnesium dissolution in iron with a drastic increase with temperature. The argument was made that during subsequent core cooling, the dissolved component should precipitate out of the core at the core-mantle boundary (CMB), providing compositional buoyancy able to drive a dynamo. This interpretation was recently challenged (Du et al., 2017), with a model of magnesium partitioning that has no temperature dependence, but depends only on the oxygen concentration in the metal. Their primary conclusion was that, while magnesium can be incorporated in the core during its formation, it remains essentially trapped during subsequent core cooling because the oxygen concentration in the core is roughly constant; hence, no magnesium exsolution would occur as a plausible buoyancy source to power a geodynamo.

The essential question raised by these conflicting reports is that of the proper thermodynamic model describing magnesium metal-silicate partitioning. While one study assumes MgO dissolution (Badro et al., 2016) into liquid metal, the other (Du et al., 2017) proposes iron-magnesium exchange. In order to effectively

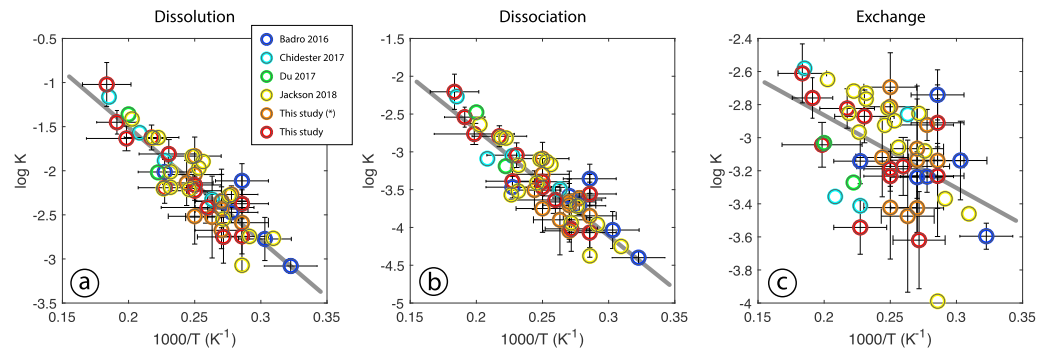


Figure 1. Search for a thermodynamically consistent model of magnesium metal-silicate partitioning. The equilibrium constants are plotted as a function of reciprocal temperature, assuming (a) dissolution (equation (5)), (b) dissociation (equation (4)), and (c) exchange (equation (6)), along with error bars propagated from analytical uncertainties (Table S1). The (a) dissolution and (b) dissociation reactions provide an excellent description of the data, where the gray fitted line has an $R^2 = 0.959$ and 0.957 , respectively. The (c) exchange reaction shows little correlation ($R^2 = 0.681$). The parameters (a and b) of the fitted black lines are given in Table S2, and all models show no resolvable pressure dependence ($c = 0$). It is noteworthy that the uncertainties (error bars plotted only for the present data + data from Badro et al., 2016) are on the same order as the scatter in the data, which is statistically self-consistent. The orange data points labeled as “This study (*)” are reanalyses of previous experiments (Blanchard et al., 2017).

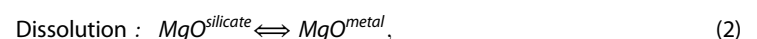
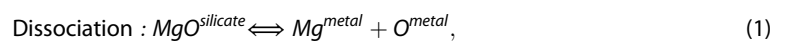
discriminate between the models and resolve this issue, an accurate and thermodynamically consistent framework is required. One such model is the interaction parameter model (Ma, 2001), that has been successfully implemented in recent metal-silicate partitioning studies (Corgne et al., 2008; Siebert et al., 2011, 2013). However, it requires a substantial data set, unavailable to date for magnesium; the extremely high temperatures required for magnesium partitioning into metal are attainable only in laser-heated diamond anvil cell experiments, explaining the scarcity of available data.

2. Experiments

Here we report 22 new experiments carried out between 34 and 138 GPa and 3,500 and 5,450 K in the laser-heated diamond anvil cell. Two series of metal-silicate equilibration experiments (see supporting information) were carried out at IPGP (Paris, France) and ELSI (Tokyo, Japan). In both cases, the samples were compressed to target pressure, equilibrated at high temperature using double-sided laser heating, temperature-quenched in several tens of microseconds, and finally decompressed. Thin sections were extracted from the center of the laser-heating spot using a focused ion beam instrument. All sections show a coalesced metal ball in the center of the sample, surrounded by quenched molten silicate (Figure S1), indicating equilibration above the liquidus temperature of both metal and silicate. The chemical composition of the metal and silicate phases (Table S1) were measured by high-resolution (FEG source) EPMA (ELSI) and EDX spectroscopy (IPGP). Some of the experiments are from Blanchard et al. (2017) and were reanalyzed using a high spatial resolution FEG probe (orange circles in Figures 1 and 2). Details about the experimental and analytical protocols can be found in supporting information. The 22 new data (including 10 reanalyzed data from Blanchard et al., 2017) were combined with the other available data sources to date: 6 experiments from Badro et al. (2016), 4 experiments from Chidester et al. (2017), 2 experiments from Du et al. (2017), and 15 experiments from Jackson et al. (2018), producing a total data set of 49 samples.

3. Thermodynamic Model

Magnesium partitioning between metal and silicate can a priori follow one of three different reactions: a *dissociation* reaction (equation (1)), a *dissolution* reaction (equation (2)), an iron-magnesium *exchange* reaction (equation (3)):



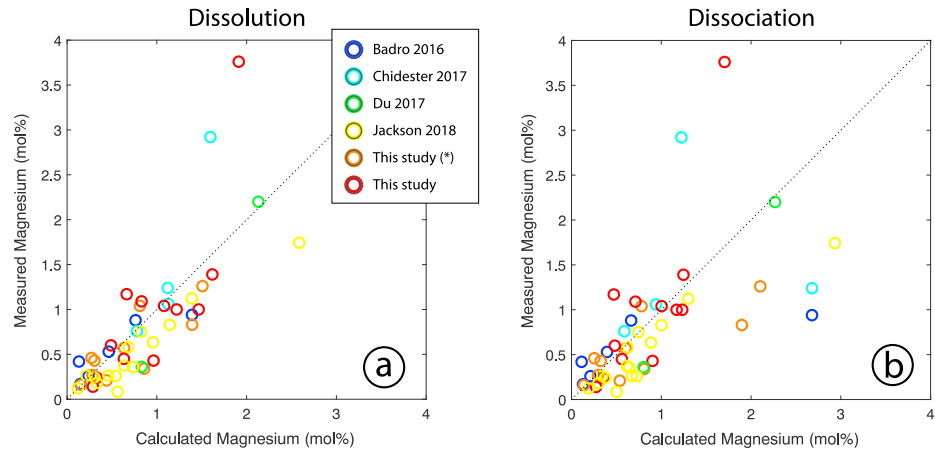


Figure 2. Comparison between measured and calculated magnesium concentrations, using the two valid (Figure 1) thermodynamic models: (a) dissolution (model in equation (9)) and (b) dissociation (model in equation (8)). The dissolution model is more accurate (fits well all but the two highest concentrations, red and light blue outliers in (a)) and was used in the main discussion. The dissociation model is considered in supporting information.

The equilibrium constant K was calculated for each of the three reactions (see supporting information). The equilibrium constant for the dissociation reaction (equation (1)) can be written as

$$\log K = \log \frac{X_{Mg}^{metal} X_O^{metal}}{X_{MgO}^{silicate}} + \log \gamma_{Mg}^{metal} + \log \gamma_O^{metal}, \quad (4)$$

that for the dissolution reaction (equation (2)) as

$$\log K = \log \frac{X_{MgO}^{metal}}{X_{MgO}^{silicate}} + \log \gamma_{Mg}^{metal} + \log \gamma_O^{metal}, \quad (5)$$

that for the exchange reaction (equation (3)) as

$$\log K = \log \frac{X_{Mg}^{metal} X_{FeO}^{silicate}}{X_{Fe}^{metal} X_{MgO}^{silicate}} + \log \gamma_{Mg}^{metal} - \log \gamma_{Fe}^{metal}, \quad (6)$$

where X_i are the molar concentration of each component in the relevant phase and γ_i are their activity coefficients in that same phase obtained using the interaction parameter formalism where the coefficients are broken down into multiple sums of interaction parameters ϵ_i^j (see supporting information). Note that in the case of dissolution (equation (5)), the activity coefficients of Mg and O are considered; because it is assumed that the dissolved MgO component further breaks down to Mg and O ions in the metal, rather than remaining covalently-bonded MgO (see supporting information and Figure S2). Therefore, while MgO is the species undergoing the reaction between metal and silicate (hence, X_{MgO} in equation (5)), the relevant activity coefficients (that depend solely on the composition of the metal alloy) should be those of Mg and O (hence, γ_{Mg} and γ_O in equation (5)).

The logarithm of each equilibrium constant is also equal to

$$\log K = a + \frac{b}{T} + c \frac{P}{T}, \quad (7)$$

where T is temperature, P is pressure, and a , b , and c are the entropy, enthalpy, and volume changes of the considered reaction, respectively (Wood, 2008).

Therefore, equations (4)–(6) can be rewritten as follows:

$$\log \frac{X_{Mg}^{metal} X_O^{metal}}{X_{MgO}^{silicate}} = a + \frac{b}{T} + c \frac{P}{T} - \log \gamma_{Mg}^{metal} - \log \gamma_O^{metal}, \quad (8)$$

$$\log \frac{X_{MgO}^{metal}}{X_{MgO}^{silicate}} = a + \frac{b}{T} + c \frac{P}{T} - \log \gamma_{Mg}^{metal} - \log \gamma_O^{metal}, \quad (9)$$

$$\log \frac{X_{Mg}^{metal} X_{FeO}^{silicate}}{X_{Fe}^{metal} X_{MgO}^{silicate}} = a + \frac{b}{T} + c \frac{P}{T} - \log \gamma_{Mg}^{metal} + \log \gamma_{Fe}^{metal}, \quad (10)$$

where the left-hand-side of the equation reflects the (measured) chemical composition, and the right-hand-side of the equation groups the T and P dependence with the unknowns: a , b , c , and activity coefficients γ_i^{metal} in the metal. These were obtained for each of the three models by ordinary least-squares linear regression of equations (8)–(10), and the parameters are reported in Table S2 and plotted along with the data in Figure 1.

While the thermodynamics of the dissociation (equation (1)) and dissolution (equation (2)) reactions show an outstanding fit to the data (R^2 of 0.959 and 0.957, respectively) and statistical significance (Table S2), that of the exchange reaction (equation (3)) yields a significantly poorer fit to the available data (R^2 of 0.681). This is clearly seen in Figure 1, where $\log K$ shows remarkable linearity with reciprocal temperature for dissociation and dissolution, and arbitrary scatter with a nonstatistically significant temperature dependence for exchange. It is not surprising for dissociation and dissolution to yield comparable results, because equations (4) and (5) are very similar, and only differ in the way oxygen is accounted for in the reactions. In the case of dissolution, it is correlated to magnesium concentration, whereas in the dissociation reaction, Mg and O concentrations are independent. These two successful models can further be compared in the way they reproduce the experimental observations (Figure 2); apart for the two highest temperature points, the dissolution model reproduces all the experimental observations, whereas the dissociation model shows more significant scatter mainly at higher MgO (and oxygen) concentrations in the metal. While our observations favor the dissolution model, more experiments (especially with varying oxygen concentrations in the metal) are needed to definitely support one model over the other.

4. Magnesium Concentration in the Core

Because there is no resolvable pressure dependence ($c = 0$ with a p value of 0.828, Table S2) of magnesium partitioning, the concentration of magnesium in the core is a function of temperature and composition only. The equilibrium molar concentration of MgO in the core (between core and mantle, at the CMB) can be obtained by rewriting equation (9) as

$$\log X_{MgO}^{core} = a + \frac{b}{T_{CMB}} + \log X_{MgO}^{mantle} - \log \gamma_{Mg}^{core} - \log \gamma_O^{core}, \quad (11)$$

where T_{CMB} is temperature at the CMB, X_{MgO}^{mantle} is the molar concentration of MgO in the mantle, and γ_{Mg}^{core} and γ_O^{core} are the activity coefficients of Mg and O in liquid iron at CMB conditions, respectively. These are calculated using the interaction parameter formalism following equations S3 and S4 (see supporting information) and depend only on temperature and metal composition. Therefore, the concentration of magnesium in the core (equation (11), left-hand term) is solely a function of CMB temperature (second right-hand term), mantle composition above the CMB (third right-hand term), and core composition below the CMB (fourth and fifth right-hand terms).

Assuming a pyrolitic mantle (50 mol% MgO) and an average (3 wt% O, 3 wt% Si) core composition (Badro et al., 2015), the equilibrium magnesium concentration in the core is plotted in Figure 3a as a function of T_{CMB} , along with uncertainties inherited from the thermodynamic model (Table S2). Its slope is the exsolution rate, plotted in Figure 3b. Note that the experimental temperature range (3,600–5,500 K, Figure 1) straddles that of T_{CMB} , so that the concentrations and exsolution rate models (Figure 3) are interpolated rather than extrapolated. The effect of core composition is discussed in supporting information; it only slightly affects equilibrium concentrations in the core and exsolution rates, and is on the same order as the uncertainties.

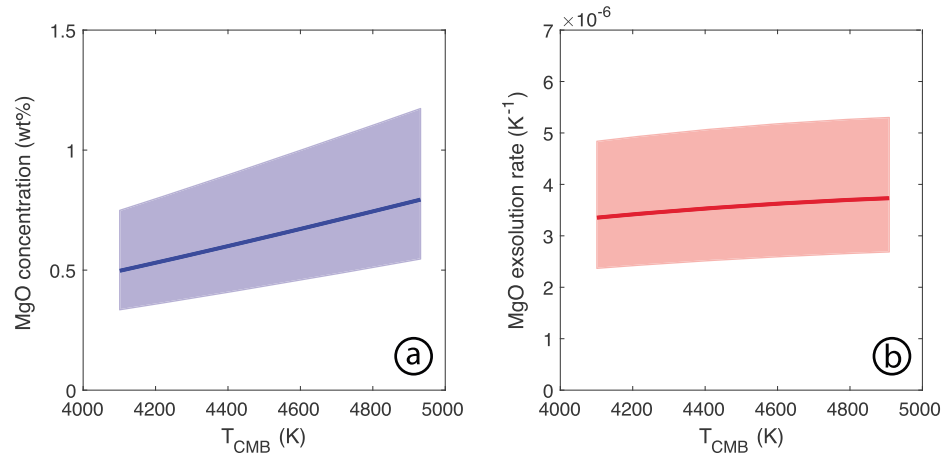


Figure 3. Equilibrium MgO concentration (a) and exsolution rate (b) in the core as a function of CMB temperature. The solid lines are the average values, and the underlying colored bands are the uncertainties propagated from the thermodynamic model (parameters and uncertainties in Table S2). This assumes an average light-element composition of the core (3 wt% O and 3 wt% Si) and an overlying mantle containing 50 mol% MgO (pyrolite). Similar plots with different compositions can be found in supporting information. CMB = core-mantle boundary.

This argues against the hypothesis that MgO exsolution is critically sensitive to the light-element composition of the core (O'Rourke & Stevenson, 2016).

5. Exsolution and the Geodynamo

The exsolution rates obtained here (Figure 3b) correspond to the lower-bound in the thermal evolution model of O'Rourke et al. (2017) that incorporates MgO precipitation in the energy and entropy balances (see supporting information). These models can in turn be used to transform the temperature dependence into time dependence and exsolution rates into mass (or buoyancy) fluxes. The evolution of CMB temperature and core cooling rate through time plotted in Figure S3 and equilibrium concentration and exsolution rates of MgO in the core (Figures 3a and 3b) are converted to a time-dependence in Figures 4a and 4b, respectively. The exsolution rate is then converted to an exsolution (buoyancy) flux at the CMB (Figure 4c), which is comprised between 2×10^4 and 10^5 kg/s. These figures are comparable to the present-day buoyancy flux (3×10^4 to 3×10^5 kg/s) due to inner-core growth (Aubert et al., 2017; Christensen & Aubert, 2006) which is the main driver of the modern geodynamo, making for a compelling case to operate an exsolution-powered geodynamo prior to inner-core growth. As in the case of inner core growth, latent heat should be released by the exsolution of MgO to the mantle. This source of energy should be however of little consequence in the present case, because it is released at the top of the core and extracted immediately to the mantle. Thus, it provides no work in the core to power a dynamo, but on the contrary a source of heat that needs to be extracted and could marginally reduce the exsolution rate.

An exsolution-driven dynamo should have the same properties as a convective dynamo driven by secular cooling, that is, by a prescribed heat flux at the CMB. This configuration has previously been shown to sustain a dipole-dominant magnetic field (Aubert et al., 2009). The RMS amplitude B_{cmb} of the magnetic field generated inside Earth's core by convection can be estimated from the buoyancy flux, through a power-based scaling law (Aubert et al., 2009; Christensen & Aubert, 2006) consistent with the intensity of the current geodynamo (see supporting information):

$$B_{CMB}^{dipole} = \beta \sqrt{\rho \mu_0} \left(\frac{\gamma g_0 F}{\rho D} \right)^{\frac{1}{3}}, \quad (12)$$

where $\rho = 10^4$ kg/m³ is the density of the outer core, $\mu_0 = 4\pi \cdot 10^{-7}$ H/m is the magnetic constant, $g_0 = 10$ m/s² is gravity at the CMB, D is outer core thickness (equal to core radius prior to inner core growth, $r_{CMB} = 3480$ km), and F is the buoyancy flux (Figure 4c) driving core convection. It has been shown (Aubert

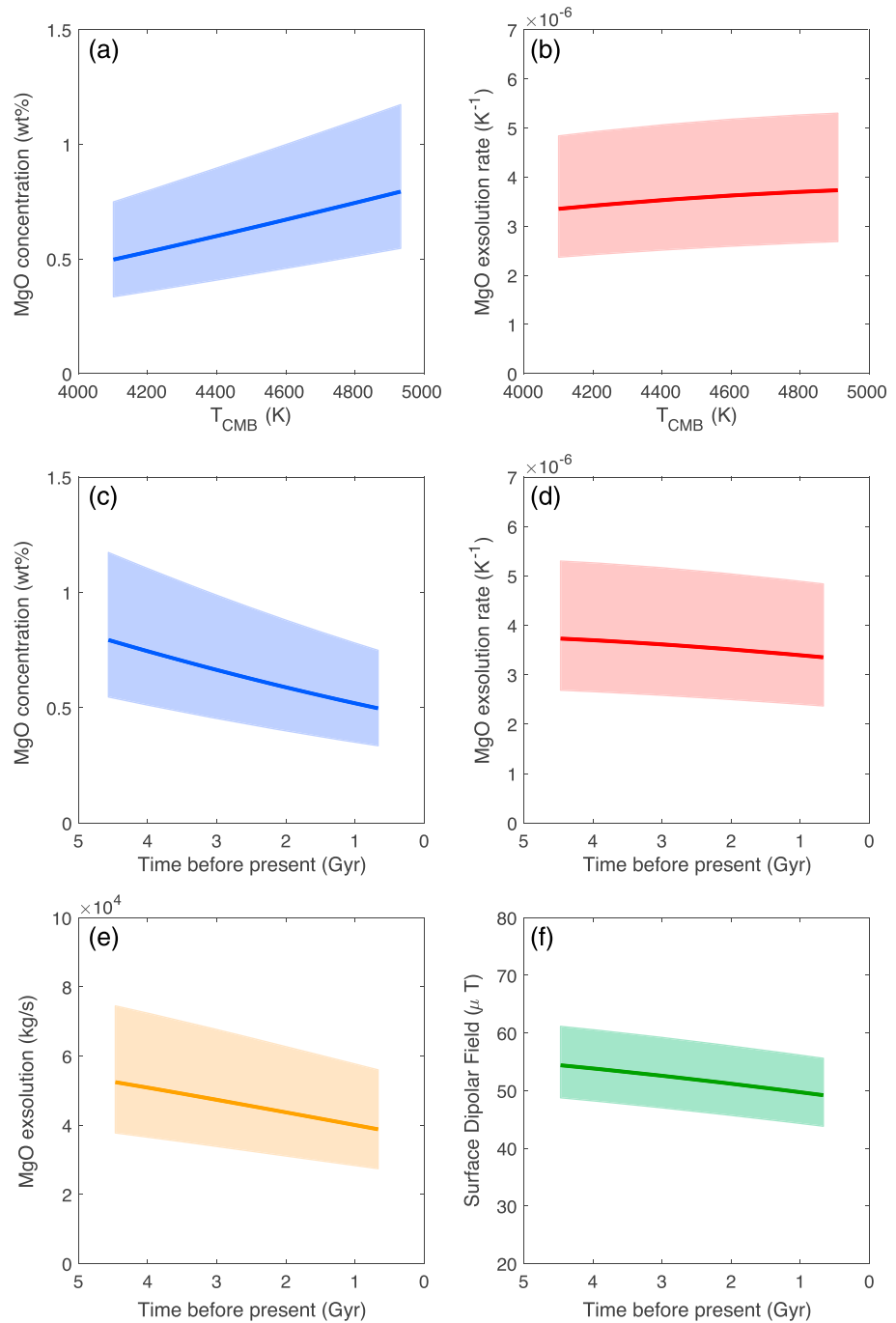


Figure 4. Equilibrium MgO concentration (a), exsolution rate (b), exsolution flux (c) in the core as a function of time, along with the dipolar magnetic field (d) produced at Earth's surface. As with Figure 3, the solid lines are obtained from the average values of the parameters in Table S2, and the underlying band are the uncertainties propagated from those parameters. (a) and (b) are the same data as Figure 3a and Figure 3b, with the x axis converted to time using the core thermal evolution model of O'Rourke et al. (2017) plotted in Figure S3. (c) Is the exsolution flux at the core-mantle boundary, which is obtained from the exsolution rate (b) and the cooling rate of the core (Figure S3). The associated dipolar magnetic field produced at the surface is obtained by converting the flux (c) using equations (12) and (13).

et al., 2009) in the thermally driven dynamo that $\gamma = 0.6$ is a geometrical factor related to the distribution of buoyancy within the core, and $\beta = 1/7$ converts the internal field in the core to dipolar field amplitude at the CMB. The RMS dipolar field intensity at Earth's surface is attenuated and scales as

$$B_{\text{surface}}^{\text{dipole}} = B_{\text{cmb}} \left(\frac{r_{\text{CMB}}}{r_{\text{Earth}}} \right)^3, \quad (13)$$

where $r_{\text{Earth}} = 6,370$ km is Earth's radius.

The intensity of the dipolar component of the exsolution-driven magnetic field at Earth's surface is plotted in Figure 4d. Intensities are comprised between 70 (4.5 Gyr ago) and 40 μT (immediately prior to inner-core growth), comparable to the present dipolar field of 40 μT that has prevailed from most of the Phanerozoic (Biggin et al., 2009) and consistent with paleointensities recorded in Proterozoic and Archean rocks dating as far back as 3.45 Ga. There could be little to no abrupt change in dipolar field intensities during the transition from that ancient exsolution dynamo prior to inner core crystallization to the modern dynamo powered by light-element release due to inner core growth. This is inline that there would also be no change in dipolar field intensity (Landeau et al., 2017) in the transition from a thermal to a buoyancy-driven dynamo at the onset of inner-core nucleation.

The onset of MgO exsolution and the initiation of the associated buoyancy-driven geodynamo is a function of the initial concentration of MgO in the core, inherited from its formation (Badro et al., 2015) and any additions due to giant impacts during accretion (Badro et al., 2016; Piet et al., 2017). If the core is oversaturated in MgO (i.e., the concentration is higher than the equilibrium concentration) at the end of core formation, MgO will precipitate out of the core until it reaches its equilibrium concentration (Figures 3a and 4a), and then follow that equilibrium concentration curve during subsequent core cooling; in this case, an MgO exsolution-driven dynamo may have operated on Earth immediately after its formation. If on the other hand the core starts out undersaturated in MgO, precipitation will only start when the temperature of the core reaches the point where its MgO concentration is equal to the equilibrium value; as the core keeps cooling and exsolution proceeds, its MgO concentration will once again follow the equilibrium concentration curve (Figures 3a and 4a). In this case, knowing the initial MgO content of the core will determine when the MgO exsolution-driven dynamo switches on.

The exsolution process described here assumes the MgO concentration in the mantle above the core is relatively constant, which supposes the mantle instantly absorbs MgO released by the core. This is certainly the case in a magma ocean regime (whether a global or a basal magma ocean), where the buoyant MgO component is immediately incorporated into and upwelled by the denser molten silicates, and should take place over a long timeframe starting at the end of Earth's accretion and core formation until the freezing of the last remnants of a basal magma ocean (Labrosse et al., 2007). Once the magma ocean atop the CMB solidifies, released MgO can accumulate as a layer at the CMB, which will significantly slow down the exsolution process (equation (11)); it will then be governed by mantle dynamics and its potential to entrain the buoyant MgO crystals away from the boundary, refreshing the silicate in contact with the core.

Our thermal evolution and magnetic intensity prediction models stop at the point where the inner core nucleates. At this onset, the cooling rate drops dramatically leaving an MgO exsolution flux on the order of a few 10^4 kg/s, which will be rapidly overcome by bottom-driven buoyancy from the core (about 3×10^5 kg/s at present). From a paleomagnetic evolution standpoint, the evolution falls back to existing post-nucleation scenarios (e.g. Aubert et al., 2009).

The geophysical implications of MgO exsolution have been discussed assuming the thermodynamics of MgO dissolution from an oxygen- and silicon-bearing core. It is striking that the geophysical implications are indistinguishable if one assumes MgO dissociation instead, or if one assumes an O-rich core or an Si-rich core, as shown in supporting information (section 5 and Figures S4–S9).

6. Conclusions

A formally correct thermodynamic framework making full use of the interaction parameter activity model shows that MgO dissolves in the metal as a function of temperature and metal composition. The model is

fully consistent with all available data to date, published (27 data) and new (22 data). On Earth, this means that dissolved MgO in the core (inherited from core formation) should precipitate out as the core cools. The exsolution fluxes are on the order of 10^4 – 10^5 kg/s which should produce a strong dipolar field at Earth's surface, on the same order as that observed today, prior to inner core growth, and potentially throughout most of Earth's history (Biggin et al., 2009; Tarduno et al., 2015; Weiss et al., 2018).

Acknowledgments

This research has received funding from the European Research Council under the European Community's Seventh Framework Programme (FP7/2007–2013) /ERC grant agreement 207467 and the JSPS research grant (KAKENHI). We acknowledge the financial support of the UnivEarthS Labex programme ANR-10-LABX-0023 and ANR-11-IDEX-0005-02. Parts of this work were supported by IPGP's multidisciplinary program PARI, and by Région Ile-de-France SESAME Grant 12015908. J.B. acknowledges support by the Green Foundation for Earth Sciences at the Institute for Geophysics and Planetary Physics, Scripps Institution for Oceanography, UC San Diego. We thank Colin Jackson and Joe O'Rourke for insightful reviews that helped improve the manuscript and Stéphane Labrosse, Dave Stegman, Bruce Buffett, John Tarduno, and Benjamin Weiss for enlightening discussions. All the data used in this paper are in Table S1, as well as in two excel spreadsheets available for download on the publisher's website as Data Sets S1–S3.

References

- Akahama, Y., & Kawamura, H. (2006). Pressure calibration of diamond anvil Raman gauge to 310GPa. *Journal of Applied Physics*, *100*(4), 043516–043514. <https://doi.org/10.1063/1.2335683>
- Andraut, D., Fiquet, G., Itie, J. P., Richet, P., Gillet, P., Hausermann, D., & Hanfland, M. (1998). Thermal pressure in the laser-heated diamond-anvil cell: An X-ray diffraction study. *European Journal of Mineralogy*, *10*(5), 931–940. <https://doi.org/10.1127/ejm/10/5/0931>
- Aubert, J., Gastine, T., & Fournier, A. (2017). Spherical convective dynamos in the rapidly rotating asymptotic regime. *Journal of Fluid Mechanics*, *813*, 558–593. <https://doi.org/10.1017/jfm.2016.789>
- Aubert, J., Labrosse, S., & Poitou, C. (2009). Modelling the palaeo-evolution of the geodynamo. *Geophysical Journal International*, *179*(3), 1414–1428. <https://doi.org/10.1111/j.1365-246X.2009.04361.x>
- Badro, J., Brodholt, J. P., Piet, H., Siebert, J., & Ryerson, F. J. (2015). Core formation and core composition from coupled geochemical and geophysical constraints. *Proceedings of the National Academy of Sciences of the United States of America*, *112*(40), 12,310–12,314. <https://doi.org/10.1073/pnas.1505672112>
- Badro, J., Siebert, J., & Nimmo, F. (2016). An early geodynamo driven by exsolution of mantle components from Earth's core. *Nature*, *536*(7616), 326–328. <https://doi.org/10.1038/nature18594>
- Biggin, A. J., Piispa, E. J., Pesonen, L. J., Holme, R., Paterson, G. A., Veikkolainen, T., & Tauxe, L. (2015). Palaeomagnetic field intensity variations suggest Mesoproterozoic inner-core nucleation. *Nature*, *526*(7572), 245–248. <https://doi.org/10.1038/nature15523>
- Biggin, A. J., Strik, G. H. M. A., & Langereis, C. G. (2009). The intensity of the geomagnetic field in the late-Archaeon: New measurements and an analysis of the updated IAGA palaeointensity database. *Earth, Planets and Space*, *61*(1), 9–22. <https://doi.org/10.1186/BF03352881>
- Blanchard, I., Siebert, J., Borensztajn, S., & Badro, J. (2017). The solubility of heat-producing elements in Earth's core. *Geochemical Perspectives Letters*, 1–5. <https://doi.org/10.7185/geochemlet.1737>
- Buffett, B. A., Huppert, H. E., Lister, J. R., & Woods, A. W. (1996). On the thermal evolution of the Earth's core. *Journal of Geophysical Research*, *101*, 7989–8006. <https://doi.org/10.1029/95JB03539>
- Chidester, B. A., Rahman, Z., Richter, K., & Campbell, A. J. (2017). Metal-silicate partitioning of U: Implications for the heat budget of the core and evidence for reduced U in the mantle. *Geochimica et Cosmochimica Acta*, *199*, 1–12. <https://doi.org/10.1016/j.gca.2016.11.035>
- Christensen, U. R., & Aubert, J. (2006). Scaling properties of convection-driven dynamos in rotating spherical shells and application to planetary magnetic fields. *Geophysical Journal International*, *166*(1), 97–114. <https://doi.org/10.1111/j.1365-246X.2006.03009.x>
- Corgne, A., Keshav, S., Wood, B. J., McDonough, W. F., & Fei, Y. (2008). Metal-silicate partitioning and constraints on core composition and oxygen fugacity during Earth accretion. *Geochimica et Cosmochimica Acta*, *72*(2), 574–589. <https://doi.org/10.1016/j.gca.2007.10.006>
- Du, Z., Jackson, C., Bennett, N., Driscoll, P., Deng, J., Lee, K. K. M., et al. (2017). Insufficient energy from MgO exsolution to power early geodynamo. *Geophysical Research Letters*, *44*, 11,376–11,381. <https://doi.org/10.1002/2017GL075283>
- Gillet, N., Jault, D., Canet, E., & Fournier, A. (2010). Fast torsional waves and strong magnetic field within the Earth's core. *Nature*, *465*(7294), 74–77. <https://doi.org/10.1038/nature09010>
- Gubbins, D., Alfe, D., Masters, G., Price, G. D., & Gillan, M. J. (2003). Can the Earth's dynamo run on heat alone? *Geophysical Journal International*, *155*(2), 609–622. <https://doi.org/10.1046/j.1365-246X.2003.02064.x>
- Jackson, C. R. M., Bennett, N. R., Du, Z., Cottrell, E., & Fei, Y. (2018). Early episodes of high-pressure core formation preserved in plume mantle. *Nature*, *553*(7689), 491–495. <https://doi.org/10.1038/nature25446>
- Japan Society for the Promotion of Science and the 19th Committee on Steelmaking (1988). *Steelmaking data sourcebook*. New York: Gordon and Breach.
- Labrosse, S. (2015). Thermal evolution of the core with a high thermal conductivity. *Physics of the Earth and Planetary Interiors*, *247*, 36–55. <https://doi.org/10.1016/j.pepi.2015.02.002>
- Labrosse, S., Herrlund, J. W., & Coltice, N. (2007). A crystallizing dense magma ocean at the base of the Earth's mantle. *Nature*, *450*(7171), 866–869. <https://doi.org/10.1038/nature06355>
- Labrosse, S., Poirier, J. P., & LeMouél, J. L. (1997). On cooling of the Earth's core. *Physics of the Earth and Planetary Interiors*, *99*(1–2), 1–17. [https://doi.org/10.1016/S0031-9201\(96\)03207-4](https://doi.org/10.1016/S0031-9201(96)03207-4)
- Landeau, M., Aubert, J., & Olson, P. (2017). The signature of inner-core nucleation on the geodynamo. *Earth and Planetary Science Letters*, *465*, 193–204. <https://doi.org/10.1016/j.epsl.2017.02.004>
- Ma, Z. (2001). Thermodynamic description for concentrated metallic solutions using interaction parameters. *Metallurgical and Materials Transactions B*, *32*(1), 87–103. <https://doi.org/10.1007/s11663-001-0011-0>
- O'Neill, H. S. C., & Berry, A. J. (2006). Activity coefficients at low dilution of CrO, NiO and CoO in melts in the system CaO–MgO–Al₂O₃–SiO₂ at 1400°C: Using the thermodynamic behaviour of transition metal oxides in silicate melts to probe their structure. *Chemical Geology*, *231*(1–2), 77–89. <https://doi.org/10.1016/j.chemgeo.2006.01.004>
- O'Rourke, J. G., Korenaga, J., & Stevenson, D. J. (2017). Thermal evolution of Earth with magnesium precipitation in the core. *Earth and Planetary Science Letters*, *458*, 263–272. <https://doi.org/10.1016/j.epsl.2016.10.057>
- O'Rourke, J. G., & Stevenson, D. J. (2016). Powering Earth's dynamo with magnesium precipitation from the core. *Nature*, *529*(7586), 387–389. <https://doi.org/10.1038/nature16495>
- Piet, H., Badro, J., & Gillet, P. (2017). Geochemical constraints on the size of the moon-forming giant impact. *Geophysical Research Letters*, *44*, 11,770–11,777. <https://doi.org/10.1002/2017gl075225>
- Pozzo, M., Davies, C., Gubbins, D., & Alfe, D. (2012). Thermal and electrical conductivity of iron at Earth's core conditions. *Nature*, *485*(7398), 355–358. <https://doi.org/10.1038/nature11031>
- Siebert, J., Badro, J., Antonangeli, D., & Ryerson, F. J. (2013). Terrestrial accretion under oxidizing conditions. *Science*, *339*(6124), 1194–1197. <https://doi.org/10.1126/science.1227923>
- Siebert, J., Corgne, A., & Ryerson, F. J. (2011). Systematics of metal-silicate partitioning for many siderophile elements applied to Earth's core formation. *Geochimica et Cosmochimica Acta*, *75*(6), 1451–1489. <https://doi.org/10.1016/j.gca.2010.12.013>

- Tarduno, J. A., Cottrell, R. D., Davis, W. J., Nimmo, F., & Bono, R. K. (2015). A Hadean to Paleoproterozoic geodynamo recorded by single zircon crystals. *Science*, *349*(6247), 521–524. <https://doi.org/10.1126/science.aaa9114>
- Tarduno, J. A., Cottrell, R. D., Watkeys, M. K., Hofmann, A., Doubrovine, P. V., Mamajek, E. E., et al. (2010). Geodynamo, solar wind, and magnetopause 3.4 to 3.45 billion years ago. *Science*, *327*(5970), 1238–1240. <https://doi.org/10.1126/science.1183445>
- Tateno, S., Sinmyo, R., Hirose, K., & Nishioka, H. (2009). The advanced ion-milling method for preparation of thin film using ion slicer: Application to a sample recovered from diamond-anvil cell. *Review of Scientific Instruments*, *80*(1), 013901. <https://doi.org/10.1063/1.3058760>
- Toplis, M. J. (2004). The thermodynamics of iron and magnesium partitioning between olivine and liquid: Criteria for assessing and predicting equilibrium in natural and experimental systems. *Contributions to Mineralogy and Petrology*, *149*(1), 22–39. <https://doi.org/10.1007/s00410-004-0629-4>
- Weiss, B. P., Fu, R. R., Einsle, J. F., Glenn, D. R., Kehayias, P., Bell, E. A., et al. (2018). Secondary magnetic inclusions in detrital zircons from the Jack Hills, Western Australia, and implications for the origin of the geodynamo. *Geology*, *46*, 427–430. <https://doi.org/10.1130/G39938.1>
- Wood, B. J. (2008). Accretion and core formation: Constraints from metal-silicate partitioning. *Philosophical Transactions of The Royal Society A*, *366*(1883), 4339–4355. <https://doi.org/10.1098/rsta.2008.0115>